

## Section 2 PROGRESS IN LASER FUSION

### 2.A Ultraviolet Experiments

In previous volumes of the LLE Review the rationale for using short wavelength lasers for fusion has been discussed. In volumes 2 and 3 some of the breakthroughs in frequency conversion technology made at LLE were presented. In this volume we discuss the initial 0.35  $\mu\text{m}$  irradiation experiments performed in support of the national inertial fusion program.

Between September and November 1980 the GDL 0.35  $\mu\text{m}$  irradiation facility became fully operational and initial experiments were performed. Modifications to the 1.054  $\mu\text{m}$  system were completed in the summer and installation of the 0.35  $\mu\text{m}$  conversion system was completed by the beginning of September. Extensive check-out work on the 0.35  $\mu\text{m}$  laser diagnostics and frequency doubling and tripling conversion tests were performed during September. Subsequently, experimental work on 0.35  $\mu\text{m}$  laser light absorption began followed by initial experiments using x-ray spectroscopy, stimulated Brillouin scattering, and plasma blow-off analysis with a Thomson parabola.

Figure 7 is a schematic layout of the ultraviolet irradiation system in its present state. The most essential elements are the conversion crystals, output energy and pulse (streak camera) diagnostics, and target focusing and viewing optics.

The expanded (130 mm diameter) infrared laser beam from GDL is frequency doubled and tripled in two 14 cm diameter type II

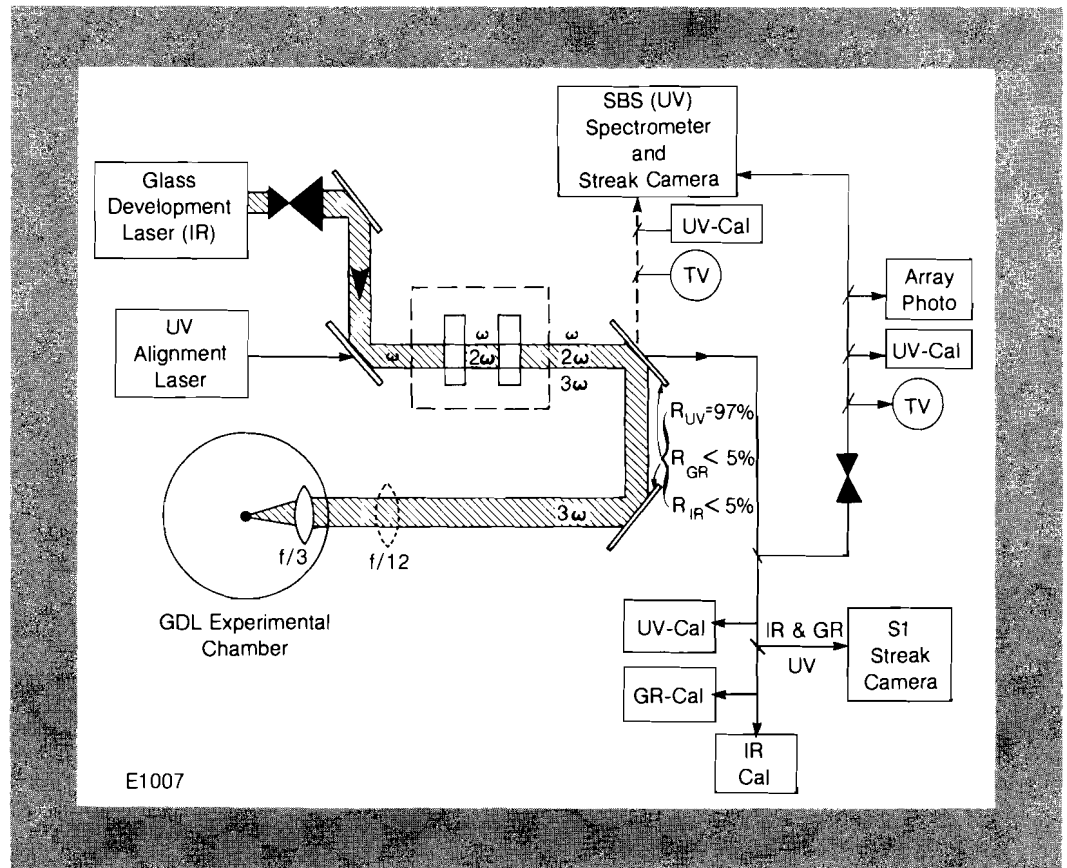


Fig. 7  
Schematic GDL-UV layout. Beam paths and diagnostics are shown for the infrared, green, and ultraviolet laser beams in GDL.

KDP crystals using a tripling scheme recently developed at LLE.<sup>1</sup> The two uncoated conversion crystals are 7.6 and 8.3 mm thick and reach maximum conversion efficiency at  $1.054 \mu\text{m}$  input intensities of approximately  $6 \text{ GW}/\text{cm}^2$ , somewhat above the present laser output capabilities of  $4 \text{ GW}/\text{cm}^2$  yielding overall energy conversion efficiencies of approximately 50 to 55% from the  $1.054 \mu\text{m}$  to  $0.35 \mu\text{m}$  output. Figure 8 illustrates predicted and measured conversion efficiencies for the present system.

UV as well as residual infrared and green output beam diagnostics are performed behind the first mirror after the crystals (see Fig. 7). This mirror reflects 97% of the UV via a second identical mirror towards the focusing optics and the target. The IR and green residual components and 3% of the UV are transmitted and their individual energies and temporal pulse shapes are measured using calorimeters and an S1 multiplexed picosecond streak camera. Typical streak camera traces are shown in Fig. 9. The UV pulse is narrower than either green or IR beams due to the lower IR-to-UV conversion efficiencies at lower power (intensity). The double-bumped IR pulse reflects the high conversion to UV at the peak of the pulse at which time the IR output pulse is significantly depleted. Intensity and time calibration for these traces are provided by calibration etalons (i.e. mirror pairs with 70% reflectivity).

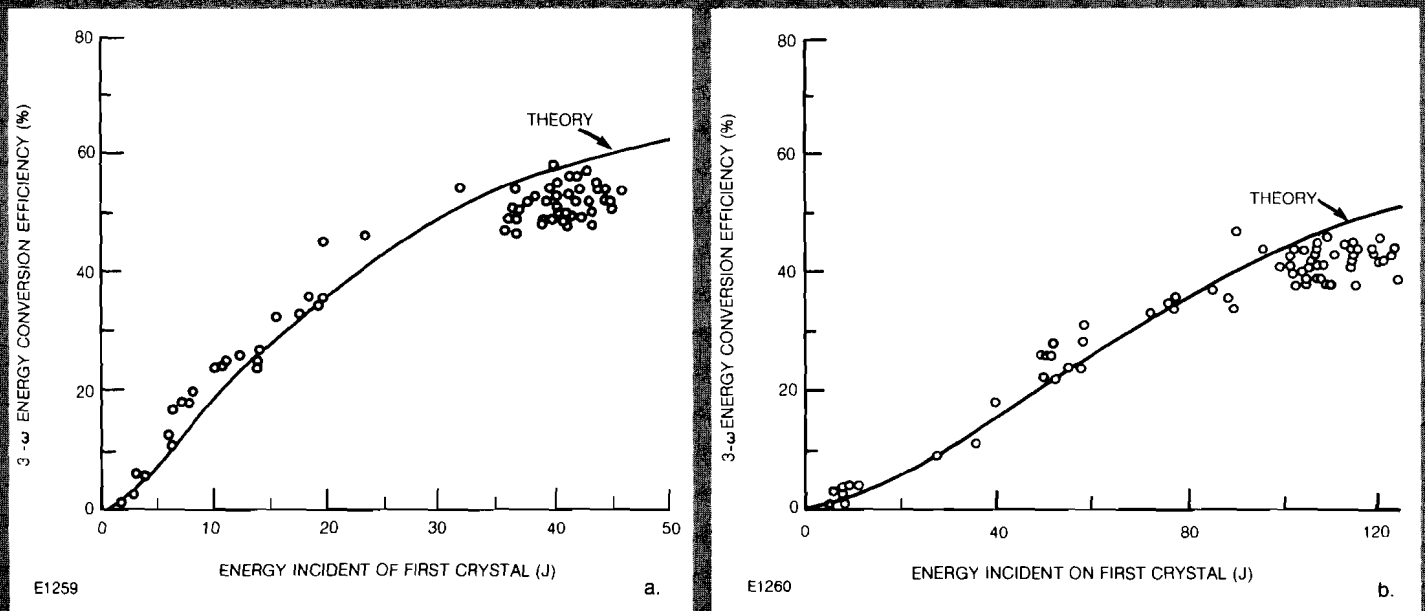


Fig. 8  
Overall  $3\omega$  energy conversion efficiencies for (a) 135 psec and (b) 600 psec IR pulses. Theoretical curves include real beam cross sections, pulse shapes, and actual crystal length (7.6 mm KDP type II doubler, 8.3 mm KDP type II tripler).

The quality (intensity distribution and collimation) of the incident IR beam and output UV beam have been characterized using near field photography and shearing-plate interferometry. A typical IR beam cross section is shown in Fig. 10 indicating intensity fluctuations in the beam of less than 10%. The beam has been collimated to less than  $\lambda/2$  in the UV. This also corresponds roughly to the uncorrectable divergence in the beam of approximately  $50 \mu\text{rad}$  leading to a minimum focus, for the f/12 focusing lens, of  $87 \mu\text{m}$  diameter. (In the future we will have at our disposal an f/2 lens with a minimum focus diameter of less than  $30 \mu\text{m}$ ).

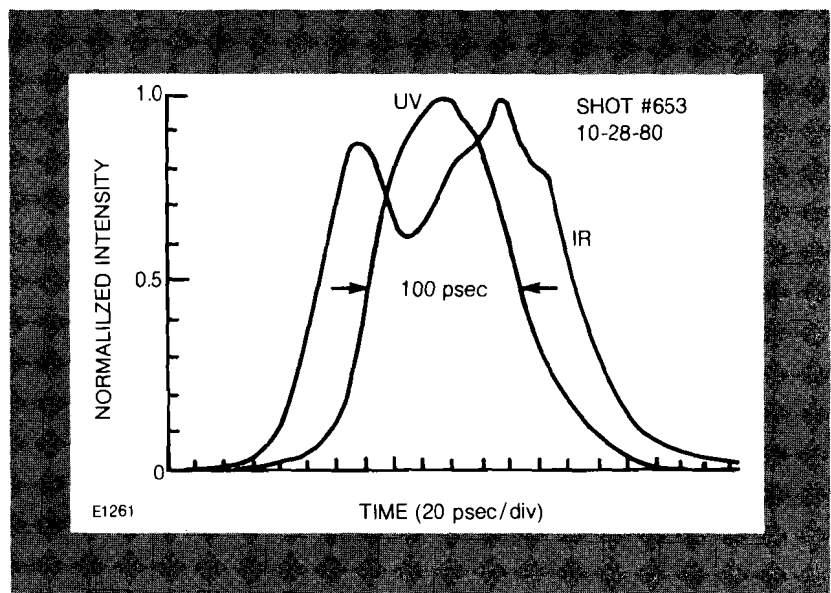
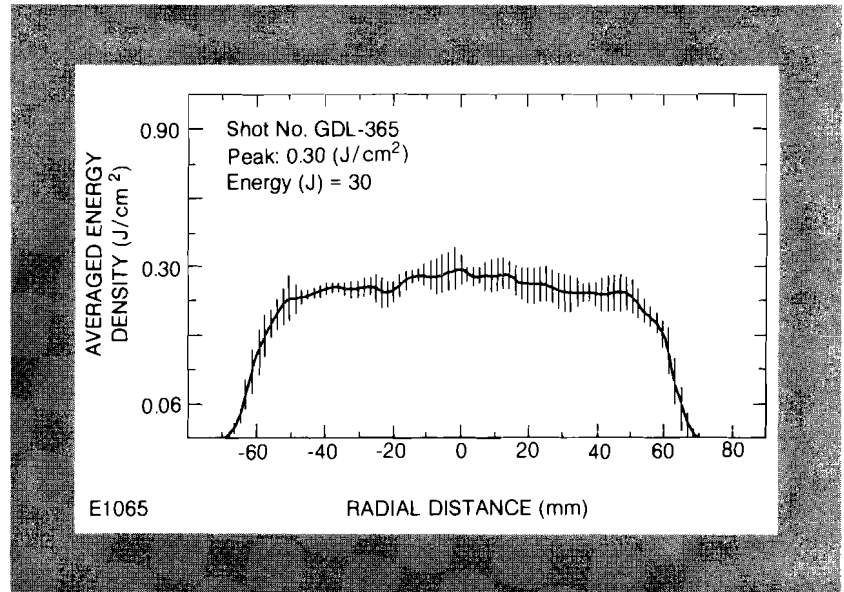


Fig. 9  
Typical streaks of IR and UV output pulses from tripler. Minimum of IR pulse is due to high tripling conversion around the peak of the pulse.

The f/2 focusing lens allows us to irradiate targets with up to  $5 \times 10^{15}$  W/cm<sup>2</sup> while the f/2 lens will raise the maximum irradiation to the  $10^{16}$  W/cm<sup>2</sup> range.

The performance of the UV irradiation facility is approximately 25 J at 100 psec and approximately 50 J at 400-500 psec - all measured in the UV. Infrared and green leakage on-target is typically below approximately  $10^{-2}$  in energy while the IR and green on-target intensity is reduced to approximately  $10^{-4}$  to  $10^{-5}$  due to the chromatic shift in the focusing lens.

Fig. 10  
Near field infrared beam cross section in front of doubling crystal. Near field photographs of the GDL infrared beam show good quality with beam intensity fluctuations of less than 10%.



The UV experimental facility has been chosen to fulfill the needs of the UV interaction program which has as its main elements:

- Absorption: measurements and evaluation of relevant absorption mechanisms
- Electron transport: determination of inhibition of free streaming electron transport and
- Hot electron generation: determination of existence and importance of hot electron generation mechanisms.

Absorption measurements are made using a box calorimeter surrounding the target. The signals from this calorimeter can be analyzed in terms of contributions arising from the scattered light and from the blow-off plasma and x-rays. The former has a short-time response while the latter has a delayed response of several minutes after the shot. The plasma and x-ray signal is due to the purely radiative coupling between the ion shield and the sensors of the box calorimeter. By analyzing both signals a redundant measurement of the absorption can be made. Linear and non-linear laser light absorption in the ion shield is avoided through the use of a quartz (Suprasil™) ion shield whose transmission at  $0.35 \mu\text{m}$  was periodically remeasured.

Between September and November 1980 the first absorption measurements were conducted. The box calorimeter yielded

results on absorption for short pulse (100 psec) irradiation between  $10^{13}$  and  $5 \times 10^{15}$  W/cm<sup>2</sup>. Some initial results have also been obtained for 400 psec pulses. We have observed absorption fractions between 60 and 95% (see Fig. 11) depending on pulse length and target material. Theoretical predictions made using 1-D (LILAC) and 2-D (SAGE) hydrocode have similar trends in the intensity dependence of the absorption and are also shown in Fig. 11.

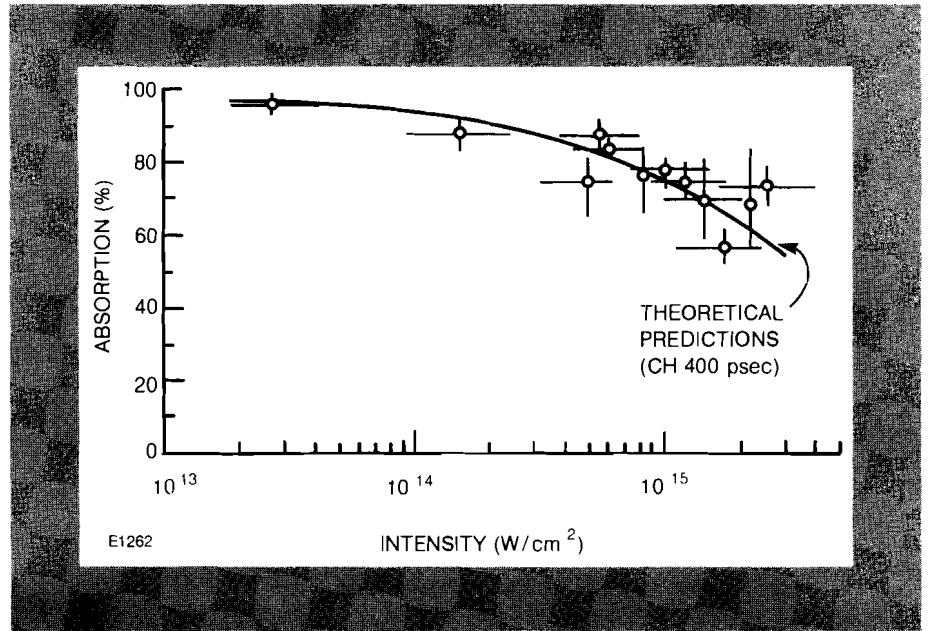


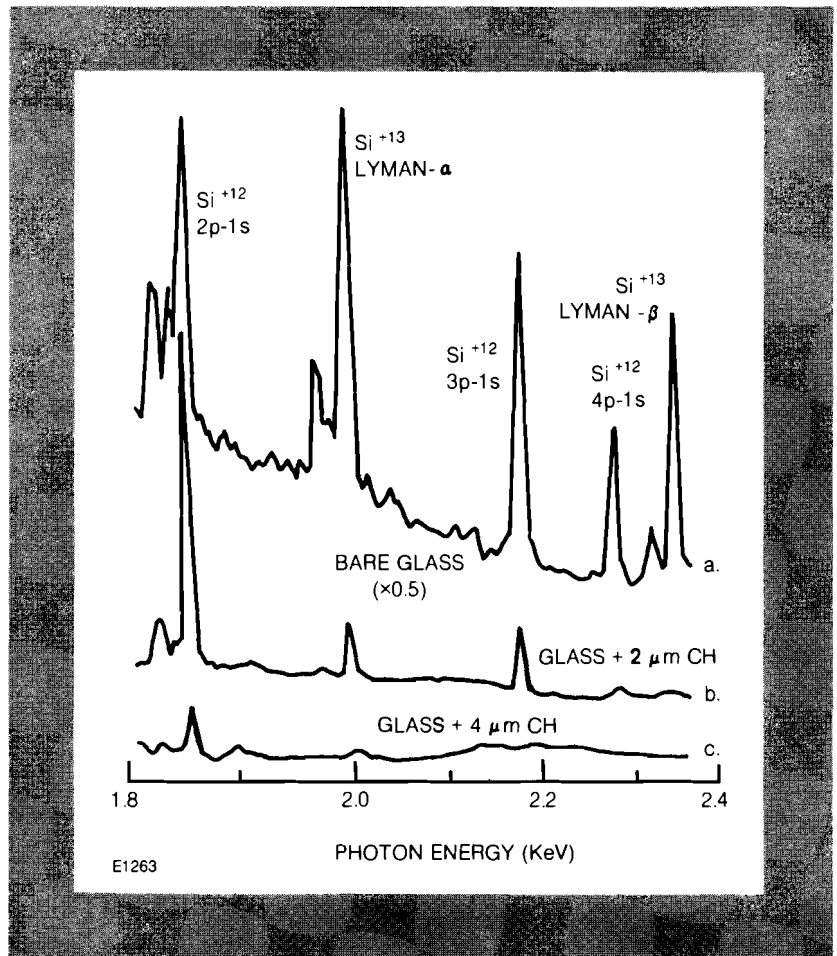
Fig. 11  
Absorption of 450 psec  $3\omega$  light by plastic targets. Dashed line is calculated absorption assuming inverse bremsstrahlung and a flux limiter of  $f=0.03$ .

X-ray spectroscopy is being used to obtain information on heat transport in the following ways:

- (a) For the plastic-coated glass targets we measure the reduction of silicon x-ray line intensity for increasing plastic thickness.
- (b) For the teflon targets we measure the intensity and Stark broadening of  $F^{+8}$ ,  $F^{+9}$  x-ray lines, both of which can be expected to increase for better heat transport into the super-dense plasma.
- (c) Ti and Ni targets can yield information on transport in high-Z plasmas. Heat inhibition produces a higher temperature and therefore enhancement of high-Z ion lines.

Figure 12 shows some examples of the results. At  $1.5 \times 10^{14}$  W/cm<sup>2</sup> (400 psec pulses) a plastic layer thickness of about  $4 \mu\text{m}$  resulted in a reduction of the silicon lines from the glass by an order of magnitude. As expected,  $\text{Si}^{+13}$  lines disappeared earlier than  $\text{Si}^{+12}$  lines. At  $2 \times 10^{15}$  W/cm<sup>2</sup> and  $2 \times 10^{13}$  W/cm<sup>2</sup>, the corresponding thickness was  $7 \mu\text{m}$  and  $1-2 \mu\text{m}$ , respectively. For 100 psec pulses at  $4 \times 10^{15}$  W/cm<sup>2</sup> that thickness was  $1-2 \mu\text{m}$ . Preliminary analysis with the 1-D laser fusion code LILAC indicates that a flux limiter  $f \sim 0.03-0.06$  is required to model the results. A more accurate analysis is underway where the intensities of these x-ray lines are calculated using a rate-dependent model including radiation transport.

Fig. 12  
 Burn-through spectra of glass targets covered with different thicknesses of plastic. X-ray spectroscopy has been used to measure the burn-through depth of plastic coated targets irradiated with a 400 psec pulse of ultraviolet. The spectra are shown for (a) bare glass target, (b) 2  $\mu\text{m}$  CH coated glass target, and (c) 4  $\mu\text{m}$  CH coated glass target. The 4  $\mu\text{m}$  CH coating reduced the intensity of the silicon line from the glass by an order of magnitude.



The results obtained from the teflon, Ti and Ni targets supplement the above measurements. The intensity of x-rays from the high-Z targets (0.12 J for the 4.7 KeV line of  $\text{Ti}^{+20}$ ), the spectral width of fluorine lines and other spectroscopic signatures are incorporated into an analysis which will yield information on the thermal transport for targets of various materials.

In the coming months experiments using time-resolved x-ray emission and absorption will be used to obtain more detailed information on absorption and transport. In addition, measurements of the continuum x-ray spectrum will be conducted to determine the importance of suprathreshold electron generation in short wavelength laser irradiation experiments.

#### REFERENCES

1. W. Seka et. al., *Opt. Comm.* **34** 469 (1980). R. Craxton, *Opt. Comm.* **34** 474 (1980).